PIV on Cavity Flame Holder in Supersonic Flow

Ho-Tse Huang, Zhi-Jun Liao, Zhong-Xuan He and Szu-I Yeh *

Department of Aeronautics and Astronautics, National Cheng Kung University, Taiwan

* siyeh@mail.ncku.edu.tw

Abstract

The primary objective of this study is to investigate the influence of the impingement location of the shear layer and cavity geometries on the distribution of recirculation zones within the cavity. Particle image velocimetry technology is employed to characterize various flow field patterns within cavities. The findings indicate that a decrease in the aft ramp angle weakens the high-speed reverse flow at the bottom of the cavity. Moreover, a lower aft ramp angle is associated with higher circulation values, promoting a more stable flow field with reduced small-scale vortex structures. The study also reveals that as length-to-depth ratio of the cavity increases, the impingement location of the shear layer and the cavity shifts towards the bottom of the cavity, leading to a weakening or disappearance of the primary recirculation zone. Concurrently, the secondary recirculation zone expands with increasing L/D, causing a notable reduction in average vorticity level and circulation value. Additionally, enhanced positive axial motion within the cavity is observed, influenced by the impingement location of the shear layer and the three-dimensional effect.

Keyword: *PIV, cavity flameholder, recirculation zone*

1. Introduction

To enhance the performance of scramjet engine, significant attention is directed towards improving fuel-air mixing capabilities and augmenting combustion efficiency. Key areas of research encompass the interaction of fuel injections in supersonic flow, structures of flow field induced by various geometric configurations, as well as the study of combustion modes, characteristics, and regimes inside the flameholder. Scholars have rigorously investigated these issues through a blend of experimental and computational approaches. Among the various proposed flameholding strategies, the cavity flameholder is considered one of the most reliable methods for providing stable ignition. Therefore, several innovative cavity-based flameholder schemes are currently being researched, including modifications to the geometric shape of the cavity flame-holder, variation of the location of fuel injection, as well as the utilization of dual cavities[1].

An ideal cavity-based flameholder is expected to possess characteristics such as lower pressure lose and drag to maximize thrust output. Furthermore, extensive research has been conducted to explore factors like residence time and fuel entrainment rate. Gruber et al.[2] used schlieren and shadowgraph flow visualizations to investigate the effects of varying parameters such as length-to-depth ratio and aft ramp angle on the flow field inside an open type cavity. The findings revealed that both decreasing the aft ramp angle and increasing length-to-depth ratio could impinge the shear layer deeper inside the cavity, leading to improved fuel entrainment rate at the expense of greater drag. Nevertheless, reducing the aft ramp angle contributed to a more stable flow field inside the cavity, making it a more optimal and reliable choice in flame holder design. Subsequent research was conducted by Zhuang et al. [3]. The findings revealed that varying ratios of length-to-depth and length-to-width yield distinct wave propagation and patterns within the cavity. Furthermore, the presence of a high-speed recirculating bubble with reverse flow was observed at the bottom of the cavity.

Although extensive research has been conducted on the flow field patterns within cavities, the distribution of recirculation zones and the dynamics of the shear layer haven't been thoroughly elucidated. A comprehensive understanding of the flow field structure within the cavity is crucial for achieving stable flame holding. Thus, the mechanisms underlying the formation of recirculation zones under varying conditions must be clarified.

In flow fields that vary dramatically, such as supersonic flow fields, the structure of the flow field could be influenced by minor pressure fluctuations within the wind tunnel. Consequently, even under identical

freestream conditions and model configuration, the captured images may differ as they represent different stages of the flow field development process. This study aims to categorize the flow field structure resulting from various flameholder configurations and identify critical flow field formations, such as shear layers and recirculation zones, through detailed velocity and vorticity analyses. Furthermore, the investigation employed the lambda2-criterion and Q-criterion methods to analyse the resulting images, facilitating the identification of vortices and shear layer regions.

2. Experimental facility and Diagnostics

2.1 Freestream condition and configuration of models

This study was conducted utilizing a reflected shock tunnel, in which helium was subjected to pressurization and heating to attain a velocity of Mach 2, with a total temperature 1700K. Three distinct cavity geometries were examined to analyze the flow field in relation to varying aft wall angles and length-to-depth ratio (L/D). The scheme and parameters associated with the cavity configurations are shown in Fig. 1and Table 1.

Table 1 Configurations of models

case	L/D	Length (mm)	Depth (mm)	Aft Wall Angle (θ)	Abbreviation
1	3	49.5 mm	16.5 mm	22.5°	LD3-AR22.5
2	3	49.5 mm	16.5 mm	18°	LD3-AR18.0
3	4	66 mm	16.5 mm	22.5°	LD4-AR22.5

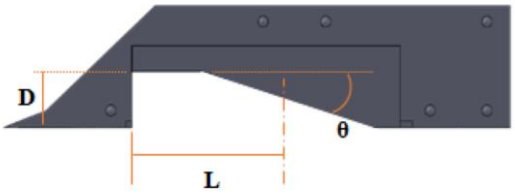

Fig. 1 Schematic diagram of cavity

2.2 PIV system

In this study, silicon dioxide (SiO2) particles with a diameter of approximately 250 nm were employed, yielding a Stokes number of 0.01289, which is below the threshold of 0.05. This value aligns with the criteria established by Samimy [4] for particle fidelity in compressible flows. The PIV apparatus utilized in the study incorporated two lasers that emitted light at staggered intervals, serving as the illumination source for the dual images captured in the PIV process. Two pulsed Nd: YAG lasers were meticulously aligned along an optical path through a series of optical mirrors, ultimately forming a light sheet that illuminated the observation area from beneath the test section of the wind tunnel, as illustrated in Fig. 2. To fulfil the analytical requirements of PIV in supersonic flow, the experiment was conducted at a resolution of 1280×800 pixels, achieving a maximum frame rate of 7500 frames per second. Additionally, an oscilloscope was employed to measure the time interval between the two laser pulses, thereby facilitating the determination of the inter-frame time necessary for PIV analysis.

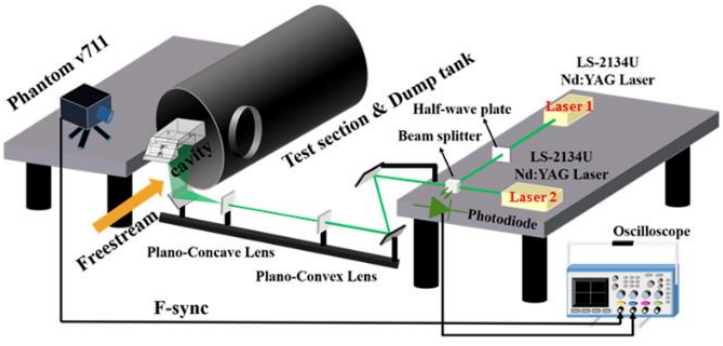

Fig. 2 PIV system

2.3 Analytical methods

This study conducts circulation analysis on the velocity field obtained from PIV calculations. Circulation analysis is then performed on these low-speed regions to analyse the flow conditions in the recirculation zone. The formula is as follows:

$$\Gamma = \oint_C \vec{V} \cdot d\vec{L} = \iint_A (\nabla \times \vec{V}) \cdot d\vec{A} \tag{1}$$

3. Results and discussion

3.1 L/D=3. Aft ramp angle=22.5 deg

The findings from the LD3-AR22.5 model reveal the existence of two distinct flow distribution patterns, as identified through extensive experimental evaluations. The first pattern is distinguished by the formation of two counterclockwise vortices, as illustrated in Fig. 3 (a). The second pattern exhibits two vortices rotating in opposite directions, as shown in Fig. 4 (a). Consistent with prior research, the counterclockwise vortex, induced by shear layer interaction with the downstream ramp, is defined as the primary vortex, while the clockwise vortex is termed the secondary vortex. For clarity and uniformity, this study refers to these flow structures as dual primary recirculation zone and single primary-secondary recirculation zone, respectively.

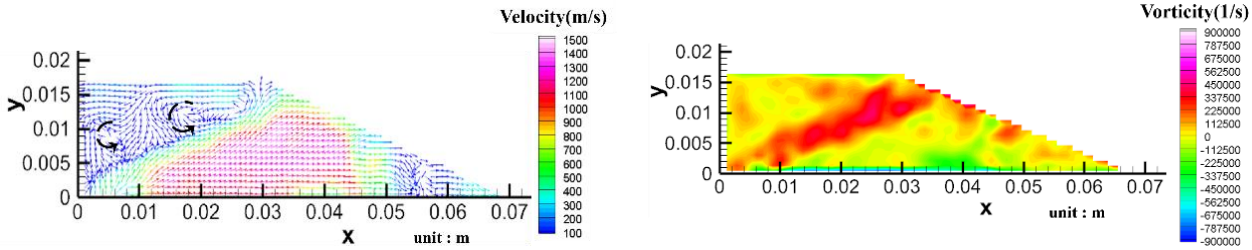

(a) Velocity distribution (b) Vorticity distribution

Fig. 3 Flow field of dual primary recirculation zone of model LD3-AR22.5

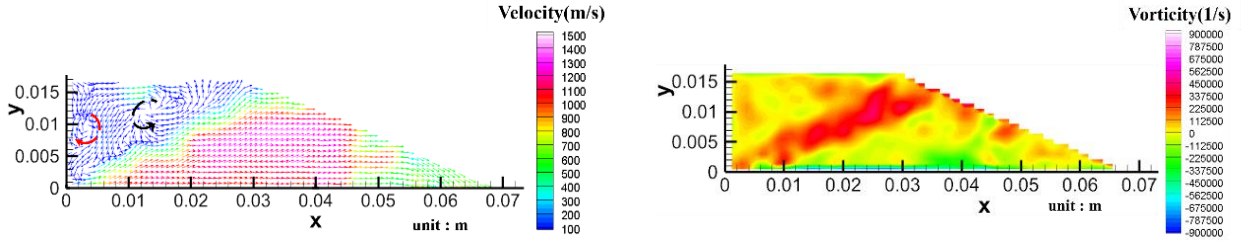

(a) Velocity distribution (b) Vorticity distribution

Fig. 4 Flow field of single primary-secondary recirculation zone of model LD3-AR22.5

Fig. 3 presents the vorticity distribution for the dual primary recirculation zone scenario of model LD3-AR22.5, where the region of peak vorticity marks the shear layer's position. Fig. 3 (a) illustrates the velocity distribution within the cavity, highlighting a high-speed reverse flow region located at (0.02, 0.013), which corresponds to the cavity's bottom. This observation aligns with the reverse flow phenomenon documented in previous studies.[5].

Fig. 4 depicts an alternative flow field configuration within the cavity of model LD3-AR22.5, referred to in this study as the single primary-secondary recirculation zone. Fig. 4 (a) identifies another distinct flow field structure emerging within the cavity. The high-speed reverse flow in this configuration amplifies the vortex strength of the primary recirculation zone, resulting in a vortex strength comparable to that observed in the shear layer region. In the study conducted by Gruber et al.[6], cavity residence time is defined as the timescale governing the mass exchange of flow within the cavity. A reduction in residence time was observed as the aft ramp angle of the cavity decreased. Configurations with lower aft ramp angles were found to generate larger primary recirculation zones, facilitating greater mass exchange compared to cavities that feature both primary and secondary recirculation zones.

The circulation analysis for the flow field derived from model LD3-AR22.5 is summarized in Table 2. Counterclockwise vortex structures exhibited positive vorticity values, while clockwise vortex structures were assigned negative values. The results indicate that cavities with dual primary recirculation zones display higher

average vorticity levels than those with single primary-secondary recirculation zones. This can be attributed to the weakening effect of the secondary recirculation zone on the vorticity strength of the primary recirculation zone, as previously noted by Gruber.

Table 2 The circulation analysis of flow field obtained from the model LD3-AR22.5

Flow field Pattern No.		Area of recirculation zone (m^2)	Average vorticity level (s^{-1})	Circulation(m^2/s)
Dual primary recirculation zone	1	152.8×10^{-6}	3.71×10^{4}	5.67
	2	165.4×10^{-6}	3.39×10^{4}	5.59
	3	168.5×10^{-6}	3.27×10^{4}	5.50
	4	167.8×10^{-6}	2.99×10^{4}	5.03
Single primary and secondary recirculation zone	5	166.0×10^{-6}	2.94×10^{4}	4.89
	6	165.1×10^{-6}	2.83×10^{4}	4.66
	7	161.8×10^{-6}	2.85×10^{4}	4.61
	8	162.3×10^{-6}	2.57×10^{4}	4.17

3.2 L/D=3. Aft ramp angle=18.0 deg

The results from model LD3-AR18.0 reveal two distinct flow patterns. The first is characterized by the presence of a single primary recirculation zone. The second pattern, as shown in Fig. 5 and Fig. 6, exhibits two vortices rotating in opposite directions and is referred to as the single primary-secondary recirculation zone.

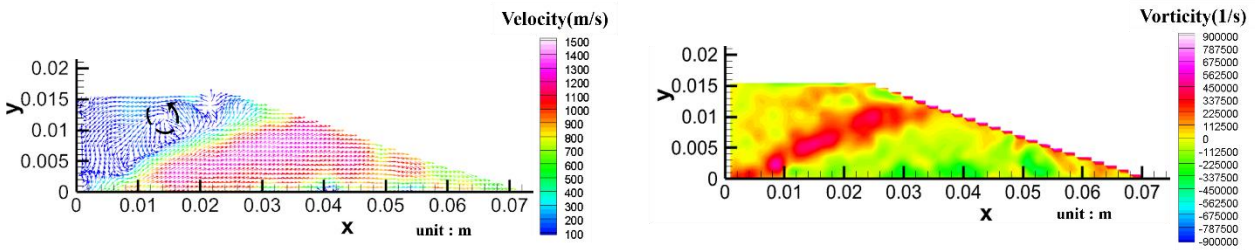

(a) Velocity distribution (b) Vorticity distribution

Fig. 5 Flow field of single primary recirculation zone of model LD3-AR18.0

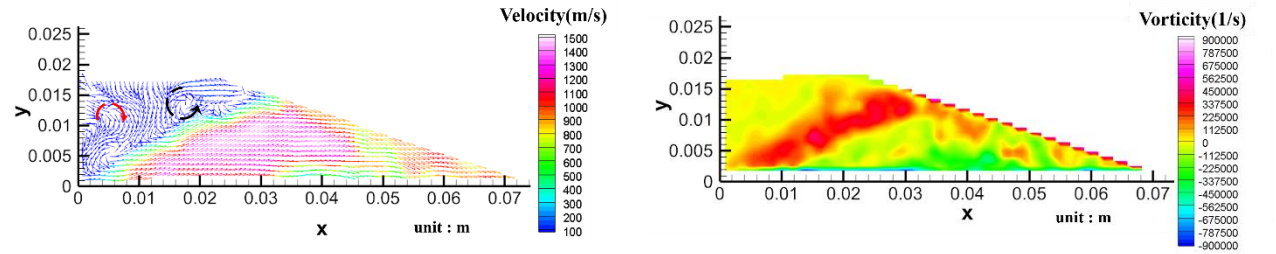

(a) Velocity distribution (b) Vorticity distribution

Fig. 6 Flow field of single primary-secondary recirculation zone of model LD3-AR18.0

In Fig. 5 (b), positive vortices are identified at coordinates (0.014, 0.012), indicating the presence of a single primary recirculation zone within the cavity. Compared to the case with a 22-degree aft ramp angle, high-speed reverse flow remains observable at the cavity's bottom; however, the vortex structure is reduced in size, and the vorticity is also weaker. This phenomenon is linked to a reduction in pressure oscillations within the cavity, which is attributed to the decrease in the aft ramp angle.

Fig. 6 (a) presents an alternative flow field pattern, where the primary and secondary vortices exhibit similar sizes. This observation is further corroborated by Fig. 6 (b), which shows a prominent negative value between the shear layer region and the front wall, highlighting the dominance of the secondary vortex in that area. Notably, unlike other cases, this flow pattern lacks the presence of high-speed reverse flow.

Table 3 presents the circulation analysis for model LD3-AR18.0. Across multiple experiments, only one instance of a single primary recirculation zone was identified. Additionally, in two cases featuring single primary-secondary recirculation zones, the average vorticity levels and circulation values were found to be comparable to those of the single primary recirculation zone case. A comparison of images reveals that the secondary vortices in these two instances are positioned closer to the front wall, indicating weaker vortex

structures. As a result, these cases exhibit smaller recirculation zone, but higher average vorticity levels and circulation values compared to cases with stronger secondary vortex strength.

Table 3 The circulation analysis of flow field obtained from the model LD3-AR18.0

Flow field Pattern	No.	Area of recirculation zone (m^2)	Average vorticity level (s^{-1})	Circulation(m^2/s)
Single primary recirculation zone	1	162.9×10^{-6}	3.74×10^{4}	6.09
Single primary and secondary recirculation zone	2	173.3×10^{-6}	3.38×10^{4}	5.88
	3	174.1×10^{-6}	3.26×10^{4}	5.70
	4	175.5×10^{-6}	2.71×10^{4}	4.76
	5	164.4×10^{-6}	2.61×10^{4}	4.29
	6	158.5×10^{-6}	2.17×10^{4}	3.45

3.3 L/D=4. Aft ramp angle=22.5 deg

The results, as shown in Fig. 7 and Fig. 8, indicate two distinct flow field patterns in this case. One pattern consists of single primary-secondary recirculation zone, while the other exhibits only single secondary recirculation zone.

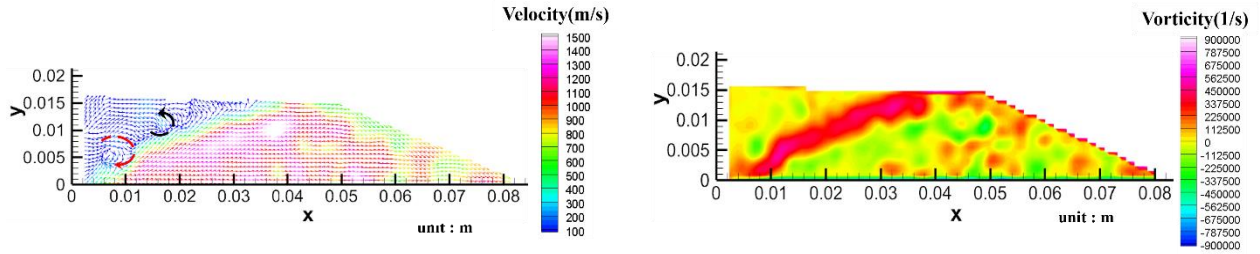

(a) Velocity distribution (b) Vorticity distribution

Fig. 7 Flow field of single primary-secondary recirculation zone of model LD4-AR22.5

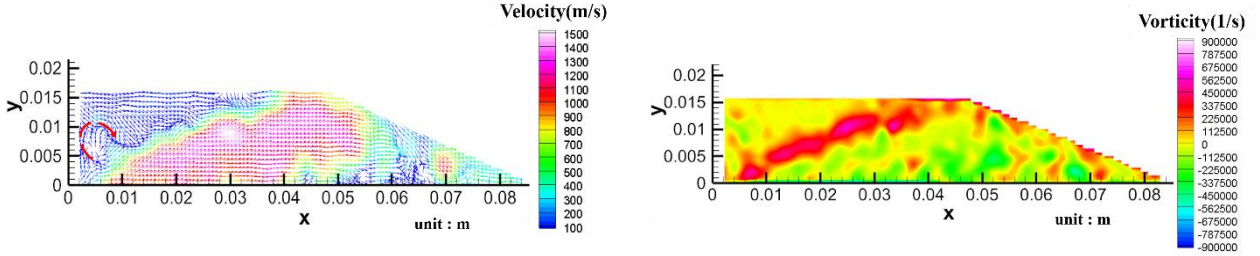

(a) Velocity distribution (b) Vorticity distribution

Fig. 8 Flow field of single secondary recirculation zone of model LD4-AR22.5

The analysis of velocity and vorticity distributions, shown in Fig. 7 (a) and (b), reveals that the primary vortex exhibits a smaller structure and lower vorticity compared to the secondary vortex. Gruber et al.[2] observed that the size of the secondary recirculation zone increases as the L/D ratio grows. However, in this study, the shear layer impingement locations on the cavity bottom under L/D = 3 and L/D = 4 conditions show no significant differences. Consequently, the enlargement of the secondary recirculation zone is noteworthy, along with a concurrent reduction in the primary recirculation zone's size due to the shear layer's influence. Fig. 8 presents an alternative flow field pattern, where the velocity distribution indicates the presence of a secondary vortex, along with a small and incomplete vortex.

Table 4 The circulation analysis of flow field obtained from the model LD4-AR22.5

Flow field Pattern	No.	Area of recirculation zone (m^2)	Average vorticity level (s^{-1})	Circulation(m^2/s)
Single primary and secondary recirculation zone	1	172.8×10^{-6}	2.49×10^{4}	4.31
	2	174.8×10^{-6}	2.42×10^{4}	4.23
	3	178.2×10^{-6}	2.22×10^{4}	3.96
	4	170.7×10^{-6}	2.15×10^{4}	3.67
Single secondary recirculation zone	5	181.2×10^{-6}	1.68×10^{4}	3.05
	6	174.3×10^{-6}	1.28×10^{4}	2.23

The circulation analysis of the flow field from model LD4-AR22.5, as presented in Table 5, shows an increasing trend in the size of the recirculation zone compared to the results from the other two models with lower L/D ratios. However, both the average vorticity level and circulation value are lower, mainly due to the reduction and eventual disappearance of the primary recirculation zone.

4. Conclusion

In this study, PIV technology and related analyses give a clearer view of the velocity field. It was found that reducing the aft ramp angle helps suppress high-speed reverse flow at the cavity bottom, which is linked to weaker pressure oscillations and compression wave strength. Results from model LD3-AR18.0 show higher circulation values. This is due to the lower aft ramp angle, which creates a more stable flow field with fewer small vortices and stronger vorticity in the recirculation zone.

Comparing the flow at different L/D ratios shows that high-speed reverse flow occurs when the shear layer hits the aft ramp, forming a compression wave and a counterclockwise vortex. As L/D increases, the shear layer impinges lower in the cavity, weakening the primary vortex and reducing high-speed reverse flow. The secondary recirculation zone expands with higher L/D, increasing vorticity near the shear layer. This leads to lower average vorticity and circulation, showing weaker overall vorticity in the cavity. At L/D = 4, stronger axial motion appears, influenced by the shear layer's position and three-dimensional effects.

This research aims to better understand how shear layer impingement and cavity geometry affect recirculation zones. Velocity field visualization offers valuable insights for improving flameholder and fuel injector designs.

References

[1] K. A. Verma, S. Kapayeva, K. M. Pandey, and K. K. Sharma, "The recent development of supersonic combustion ramjet engines for augmentation of the mixing performance and improvement in combustion Efficiency: A review," *Materials Today: Proceedings*, vol. 45, pp. 7058-7062, 2021.

[2] M. Gruber, R. Baurle, T. Mathur, and K.-Y. Hsu, "Fundamental studies of cavity-based flameholder concepts for supersonic combustors," *Journal of Propulsion and power*, vol. 17, no. 1, pp. 146-153, 2001.

[3] N. Zhuang, F. Alvi, and C. Shih, "Another Look at Supersonic Cavity Flows and Their Control," in *11th AIAA/CEAS Aeroacoustics Conference*, (Aeroacoustics Conferences: American Institute of Aeronautics and Astronautics, 2005.

[4] M. Samimy and S. K. Lele, "Motion of particles with inertia in a compressible free shear layer," *Physics of Fluids A: Fluid Dynamics*, vol. 3, no. 8, pp. 1915-1923, 1991.

[5] S. Etheridge, J. G. Lee, C. Carter, M. Hagenmaier, and R. Milligan, "Effect of flow distortion on fuel/air mixing and combustion in an upstream-fueled cavity flameholder for a supersonic combustor," *Experimental Thermal and Fluid Science*, vol. 88, pp. 461-471, 2017.

[6] G. Choubey, Y. Devarajan, W. Huang, K. Mehar, M. Tiwari, and K. Pandey, "Recent advances in cavity-based scramjet engine-a brief review," *International Journal of Hydrogen Energy*, vol. 44, no. 26, pp. 13895-13909, 2019.